

# Layer-separated distribution of nitrogen doped graphene by wrapping on carbon nitride tetrapods for enhanced oxygen reduction reaction in acid medium

Sreekuttan M. Unni <sup>a,b</sup>, Rajith Illathvalappil <sup>a</sup>, Pranav K. Gangadharan,<sup>a</sup> Siddheswar N. Bhangé<sup>a</sup> and Sreekumar Kurungot <sup>a,b</sup> \*.

## Experimental

**Graphene oxide (GO) synthesis:** In a typical synthesis, a mixture of graphite flakes and potassium permanganate (KMnO<sub>4</sub>) was slowly added to the 9:1 mixture of con. sulphuric acid (H<sub>2</sub>SO<sub>4</sub>) and phosphoric acid (H<sub>3</sub>PO<sub>4</sub>). The mixture was stirred for 12 h at 60 °C. After cooling to room temperature, deionised water (DI water) was added to dilute the mixture followed by the addition of 30% hydrogen peroxide (H<sub>2</sub>O<sub>2</sub>) to remove unreacted manganese oxide. While adding the peroxide into the acid mixture, the original pink colour of the mixture turned to yellow. The resulting solution was washed several times with nitric acid (HNO<sub>3</sub>), hydrochloric acid (HCl) and ethanol. pH of the solution was reduced using continuous washing with DI water till the pH reaches above 4. The resulting reddish brown viscous solution was washed with diethyl ether and kept for drying at a temperature of 60 °C in vacuum oven.

**Preparation of CN<sub>x</sub> wrapped nitrogen doped graphene (CNG):** CNG with different NG loading was synthesised using a simple scalable approach. In a typical synthesis, washed melamine foam was dipped in the GO solution (4 mg/ml) followed by drying using an IR lamp. For different loading of GO in the melamine foam, the number of dipping was changed. Dried GO-melamine foam was annealed at 900 °C for 3 h in argon atmosphere. The

samples are designated as CNG-1, CNG-3 and CNG-6 based on the dipping numbers of the melamine foam in the GO solution as 1 dip, 3 dips and 6 dips, respectively.

**Preparation of nitrogen doped graphene (Bulk NG):** Bulk NG was synthesised using a reported procedure. In brief, GO was mixed well with melamine powder followed by annealing at 900 °C for 3 h under argon atmosphere.

**Material Characterization:** High resolution transmission electron microscopic (HR-TEM) images were recorded using FEI Technai G2 T30 instrument operated at 300 kV. Scanning electron microscopic analysis was carried out using Quanta 200 3D FEI instrument. Raman analysis was performed in LabRam spectrometer (HJY, France) with a laser wavelength of 632 nm. X-ray photoelectron spectroscopic analysis was carried out in VGMicrotech Multilab ESCA 3000 spectrometer employing a monochromatic Mg  $K_{\alpha}$  X-ray source ( $h\nu = 1253.6$  eV). Surface area of all the samples was measured by Brunauer-Emmet-Teller (BET) nitrogen adsorption-desorption experiment on a Quantachrome Quadrasorb automatic volumetric measurement system at 77 K using ultra pure nitrogen gas.

**Electrochemical Measurements:** All the electrochemical measurements were carried out in a Biologic electrochemical workstation (VMP3) using conventional a three-electrode set-up. 0.1 M  $\text{HClO}_4$  was used as the electrolyte for the electrochemical measurements. Catalyst coated glassy carbon rotating ring-disc (Pine Instruments. Inc.) and Ag/AgCl were used as the working electrode and reference electrode, respectively. Potentials given in the manuscript are converted to reference hydrogen electrode scale using an equation,  $E_{\text{RHE}} = E_{\text{Ag/AgCl}} + 0.196 + 0.059 \text{ pH}$ . To avoid Pt contamination in the working electrode during the potential cycling, a graphite rod was used as the counter electrode. Catalyst ink was prepared by ultrasonically mixing 10 mg catalyst in 2 ml 2:3 ethanol-water mixture for 1 min. 10  $\mu\text{l}$  of the catalyst slurry was drop coated on the glassy carbon electrode, which was polished using

0.05  $\mu\text{m}$  polishing alumina powder. After drying the ink under an IR lamp, 1  $\mu\text{l}$  of 0.01 wt. % Nafion solution in ethanol was applied on the catalyst. The catalyst loading in the electrode is 0.255  $\text{mg cm}^{-2}$ . For the comparison purpose, the study was also carried out using commercial Pt/C (20 wt.% from Johnson Matthey (Alpha Acessar)) . 10 mg of Pt/C was mixed well with 2 ml of 2:3 ethanol-water mixture to prepare the catalyst ink. 5  $\mu\text{l}$  of the resulting ink was applied on the glassy carbon electrode in order to get a Pt loading of 25.5  $\mu\text{g}_{\text{Pt}} \text{cm}^{-2}$ . Cyclic voltammograms of the samples were recorded in 0.1  $\text{HClO}_4$  solution with 5  $\text{mV s}^{-1}$  scan rate in a potential window of -0.2 to 1 V vs. Ag/AgCl. Linear sweep voltammograms (LSV) were recorded using a rotating ring-disk electrode (RRDE, 0.283  $\text{cm}^2$ , Pine Instruments) at room temperature with a scan rate of 5  $\text{mV s}^{-1}$  at different electrode rotation speeds in oxygen saturated 0.1 M  $\text{HClO}_4$  electrolyte. The ring potential was kept constant at 1.2 V. For the durability and methanol tolerance tests, samples were coated on a glassy carbon electrode (0.196  $\text{cm}^2$ , Pine Instruments) and the measurements were done in 0.1 M  $\text{HClO}_4$  at a scan rate of 5  $\text{mV s}^{-1}$  with an electrode rotation speed of 1600 rpm.

Number of electron transfer and peroxide percentage were determined on the basis of the RRDE voltammogram using the following equations:

$$\frac{I_r}{I_d} = N \cdot \frac{\alpha}{1 - \alpha} \quad \text{..... (1)}$$

$$\frac{I_r}{I_d} = N \cdot \frac{\alpha}{1 - \alpha} \quad \text{.....(2)}$$

where  $I_d$  is the disc current,  $I_r$  is the ring current, and  $N$  is the collection efficiency of the Pt ring (0.37). Accelerated durability test (ADT) was performed for 5000 cycles to study the electrochemical stability of the catalyst (CNG-3). CV was performed at 100  $\text{mV s}^{-1}$  scan rate

in between a potential window of 0.7 to 1.3 V under oxygen purging. LSV was taken before and after ADT at 1600 rpm with a scan rate of  $5 \text{ mV s}^{-1}$ .

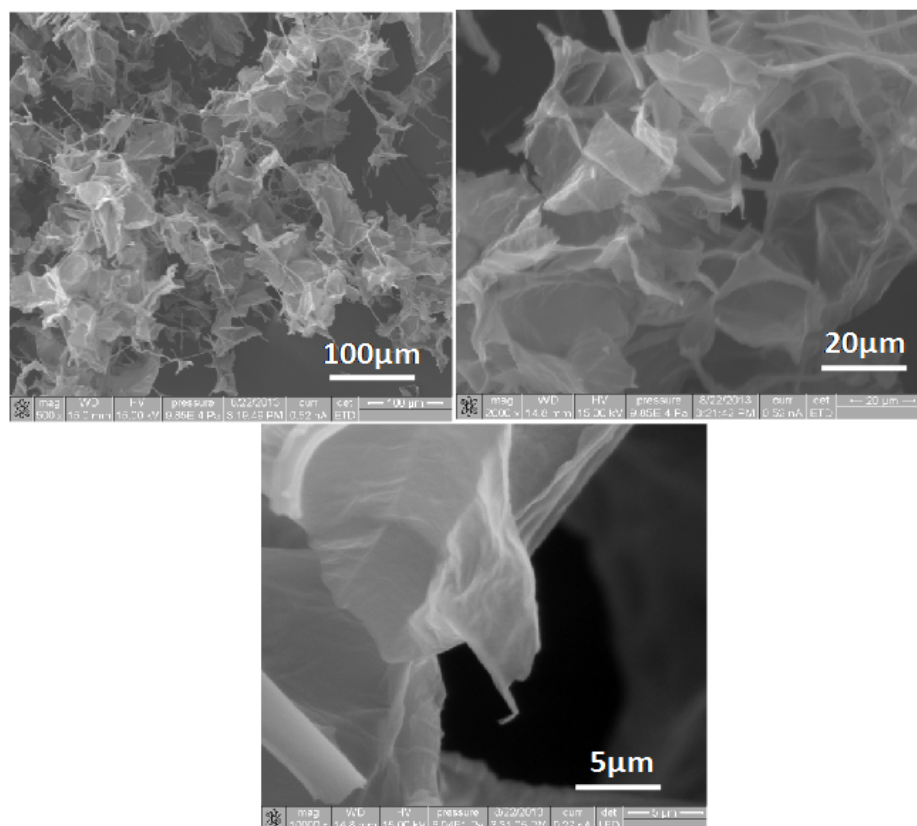


**Figure SI 1.** FE-SEM images of CNG-3 at different magnifications.

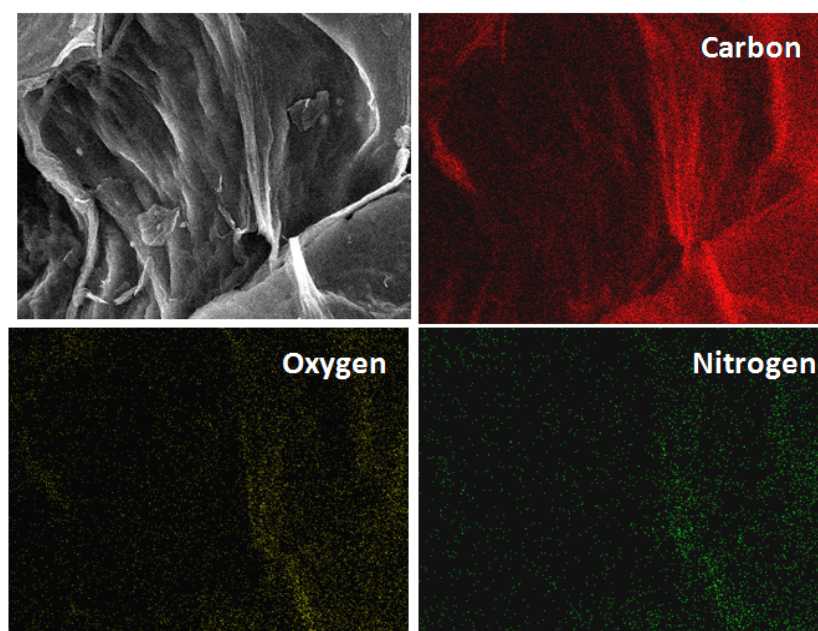


**Figure S2.** Elemental mapping of carbon, oxygen and nitrogen respectively on CNG-3.

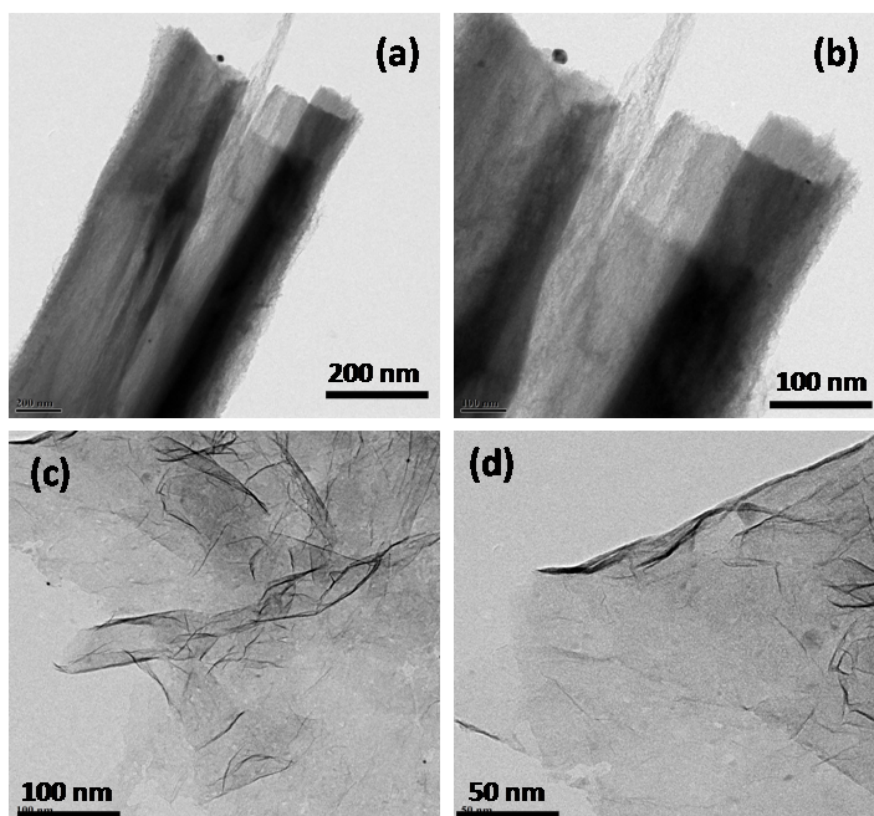


**Figure SI 3.** TEM images of CNx tetrapod scraps (a and b) and nitrogen doped graphene (c and d) of CNG-3 at different magnifications.

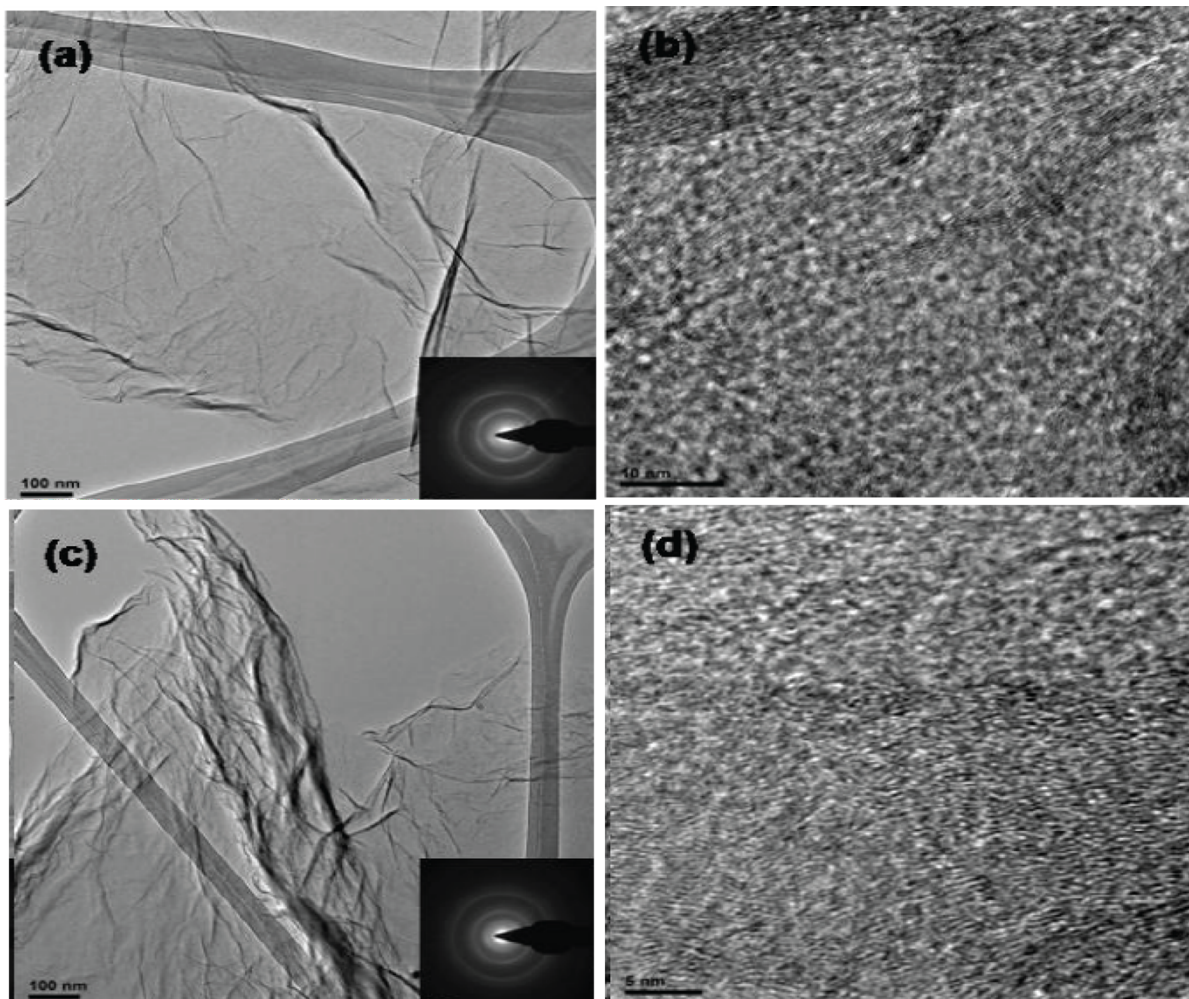


**Figure SI 4.** TEM images of nitrogen doped graphene in CNG-3 (a and b) and CNG-6 (c and d) at different magnifications.

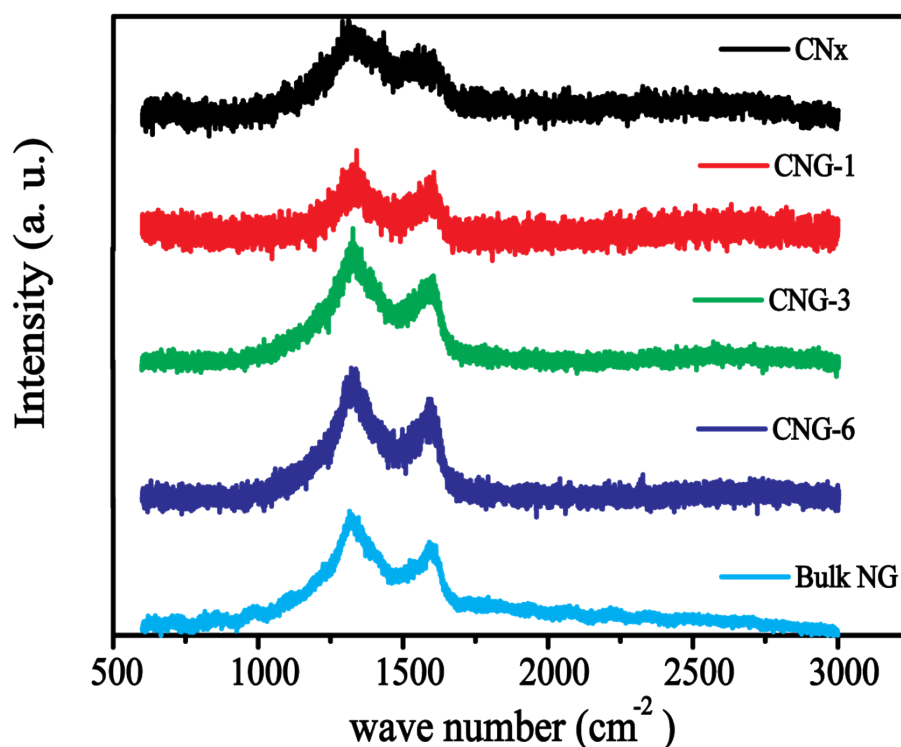


**Figure SI 5.** Raman spectra of  $\text{CN}_x$ , CNG-1, CNG-3, CNG-6 and bulk NG.

Raman spectroscopic analyses further confirm the nitrogen doping and defects created by nitrogen on CNG during the high temperature annealing. In **Figure S5**,  $\text{CN}_x$  displays the D-band at  $1318.19 \text{ cm}^{-1}$  and the G-band at  $1558.07 \text{ cm}^{-1}$ . The down shift of the G-band from  $1581 \text{ cm}^{-1}$  (of graphite) indicates that the thermally annealed MF lacks proper  $\text{sp}^2$  carbon coordination compared to the CNG samples. For the comparison purpose, bulk NG sample also was prepared separately by annealing GO and melamine mixture at  $900 \text{ }^\circ\text{C}$ . Bulk NG shows the G-band at  $1600.26 \text{ cm}^{-1}$  with up shift in the G-band position compared to the G-band position of graphite, which gives a clear evidence for n-type doping of nitrogen in the graphene sheets with defects. Compared to  $\text{CN}_x$  and bulk NG, the G-band positions of CNG-

1 (1591.10  $\text{cm}^{-1}$ ), CNG-3 (1593.03  $\text{cm}^{-1}$ ), CNG-6 (1594.24  $\text{cm}^{-1}$ ) are closer to that of pure graphite. Up shift in the peak position also confirms the nitrogen doping in the CNG samples. The shifting of the peak position towards the high wave number with increase in the dipping number indicates the defects created by nitrogen moieties are different in the CNG samples. The ratio of the D-band and G-band ( $I_D/I_G$ ) further helps to understand the chemical modifications occur during the high temperature annealing process.  $\text{CN}_x$ , bulk NG, CNG-1, CNG-3 and CNG-6 show an  $I_D/I_G$  ratio of 1.39, 1.46, 1.09, 1.49 and 1.67, respectively. CNG-3 and bulk NG have almost similar  $I_D/I_G$  ratio, indicating the presence of similar defective sites on both the materials. However, the  $I_D/I_G$  ratio is increasing with increase in the NG loading of the CNG samples, which clearly indicates that the defective sites are getting modified when the NG sheets are wrapped along the  $\text{CN}_x$  tetrapods. This may seriously affect the adsorption of dioxygen molecule and its reduction on the CNG samples. The in plane crystalline size ( $L_a$ ) ( $L_a$  is inversely proportional to the  $I_D/I_G$  ratio) of bulk NG and CNG-3 is almost same but it is decreasing with increase in the NG loading on the CNG samples. This indicates that the total nitrogen content is varying with respect to the NG sheets in the CNG samples and simultaneously defective sites in the CNG samples are also varying. Further evidence for the crystalline nature of the CNG samples has been obtained from X-ray diffraction (XRD) analysis (**Figure S6**). XRD analysis again confirms the amorphous behavior of  $\text{CN}_x$  and crystalline nature is progressively improving by the wrapping of the NG sheets on  $\text{CN}_x$ . It is evidenced from the XRD peak at  $2\theta = 26^\circ$ .

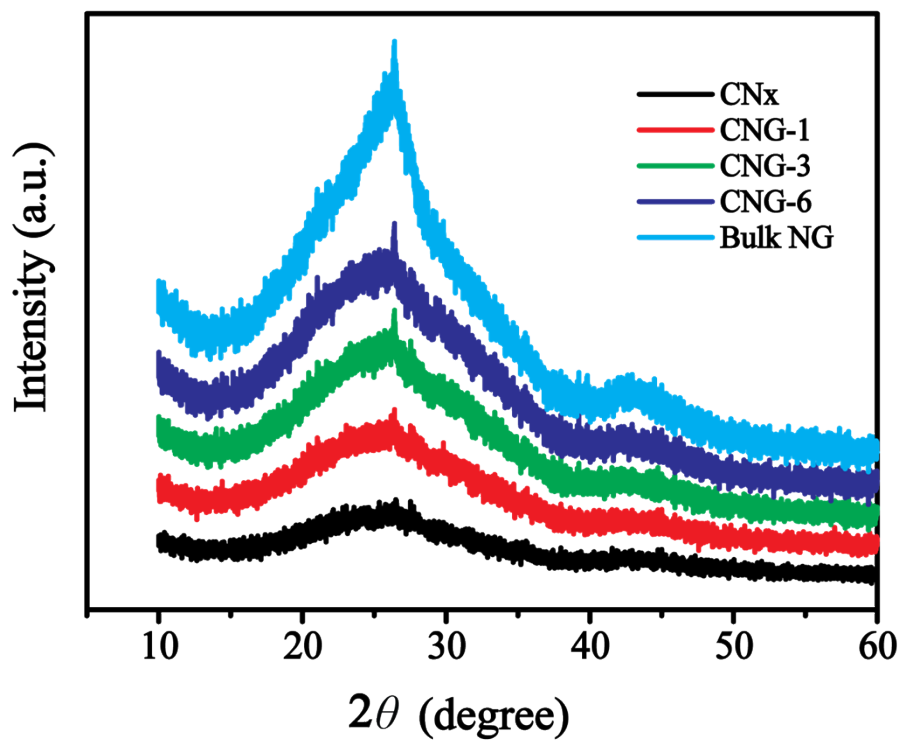


**Figure SI 6.** X-ray diffraction patterns of CN<sub>x</sub>, CNG-1, CNG-3, CNG-6 and Bulk NG sheets.

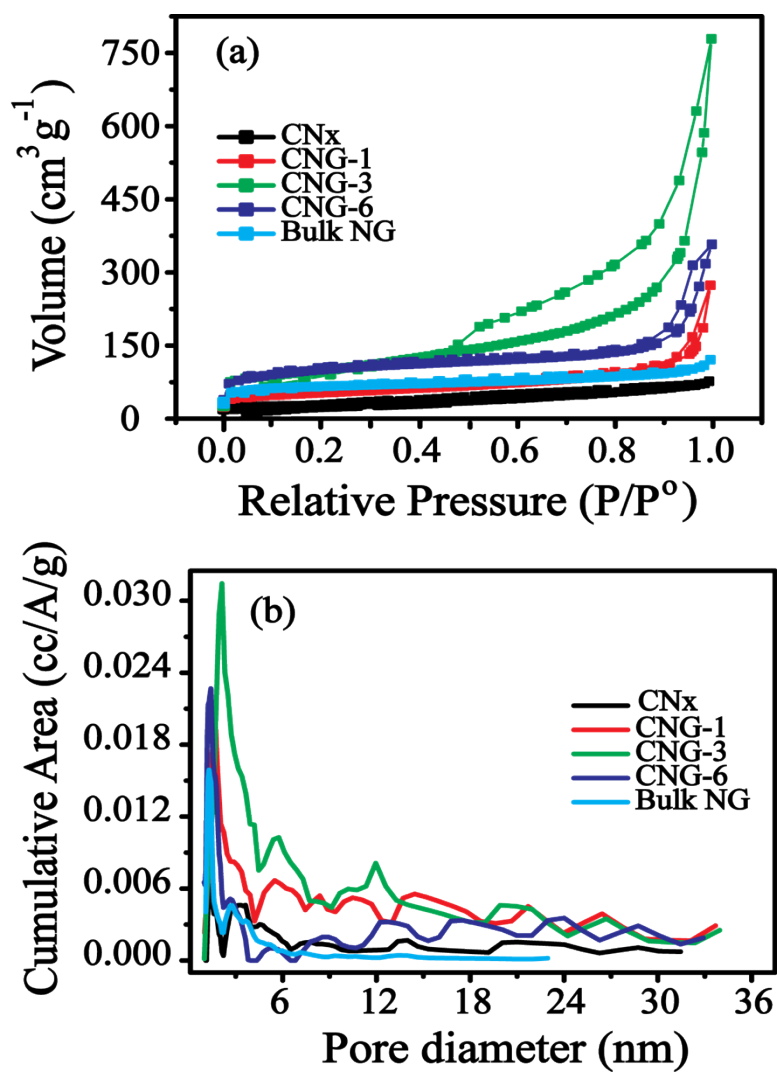


**Figure SI 7.** (a) Nitrogen adsorption–desorption isotherms and (b) pore size distribution profiles of CNx, CNG-1, CNG-3, CNG-6 and Bulk NG.

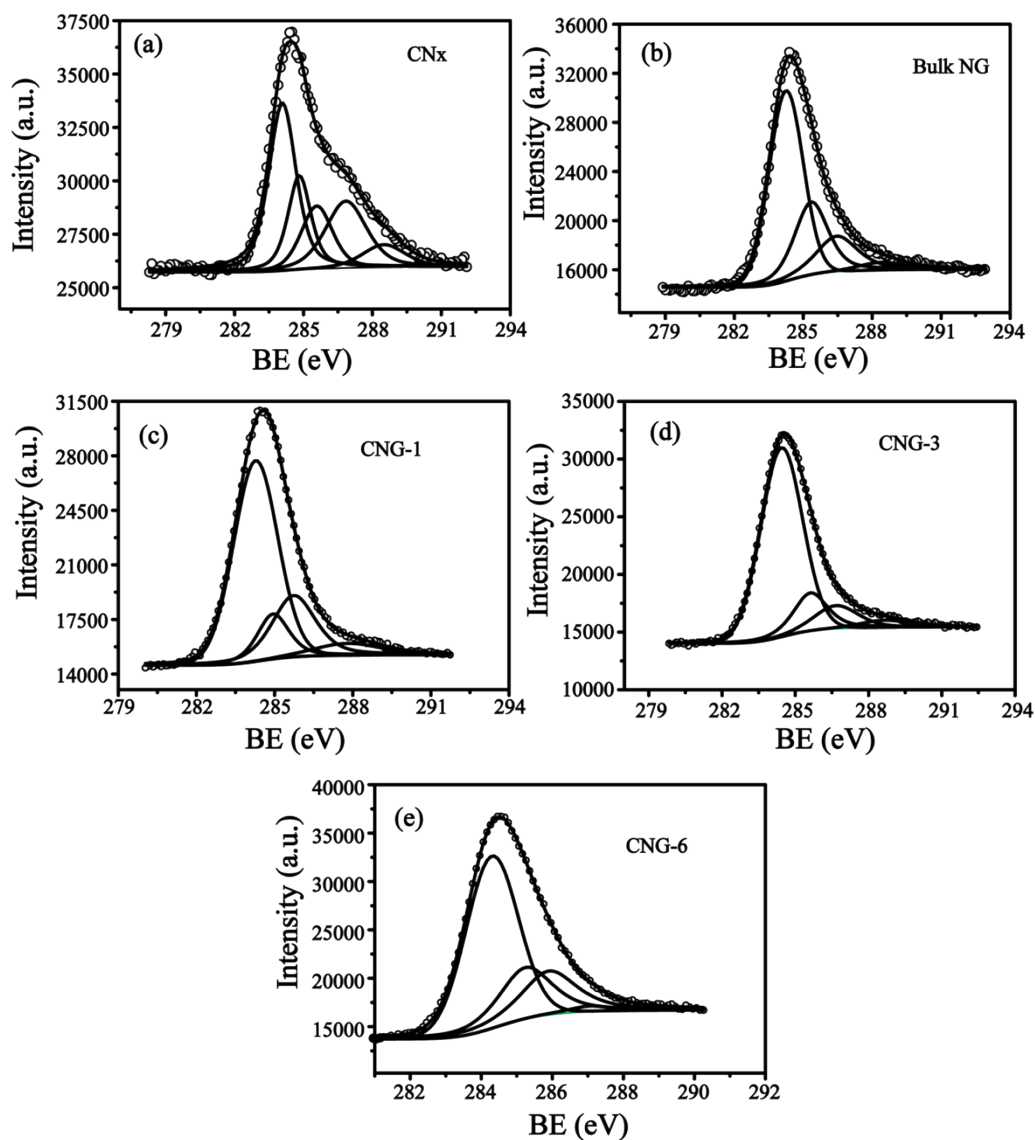


**Figure SI 8.** Deconvoluted C1s XPS spectra of (a) CN<sub>x</sub>, (b) bulk NG, (c) CNG-1, (d) CNG-3 and (e) CNG-6 samples.

Deconvoluted C1s spectra (**Figure S8**) of CN<sub>x</sub> show five distinct binding energy contributions which are indexed as 284.23 (-C=C-), 284.88 (-C-C-), 285.64 (-C-N), 286.82 (-C-O) and 288.59 eV (-C=O). High percentage of -C-C- and -C-O reduces the degree of graphitization of CN<sub>x</sub> and it is evidenced also from the Raman and XRD analyses. The peak at the binding energy of 284.31 eV of C 1s spectra of bulk NG indicates the improved graphitization of the NG sheets and the binding energy at 285.38 eV further confirms the

nitrogen doping in the sample. All the CNG samples possess improved graphitization as evidenced from the peak corresponding to the binding energy of 284.36 eV. Similarly, nitrogen doping also has been confirmed from the binding energy peak at around 285.00 eV. The wt.% of carbon is in the order of  $CN_x$  (74.26 %) < CNG-3 (80.35 %) < CNG-1 (80.54%) < Bulk NG (84.71 %) < CNG-6 (85.75 %). More interestingly, the C/O ratio of the CNG samples is increasing with increase in the NG content. The C/O ratio follows the order of  $CN_x$  (3.02) < CNG-1 (4.59) < CNG-3 (4.78) < CNG-6 (8.03) < Bulk NG (9.52). Lower C/O ratio of CNG-1 and CNG-3 compared to CNG-6 further gives evidence of thin layer coating of the NG sheets on the  $CN_x$  backbone for both CNG-1 and CNG-3.

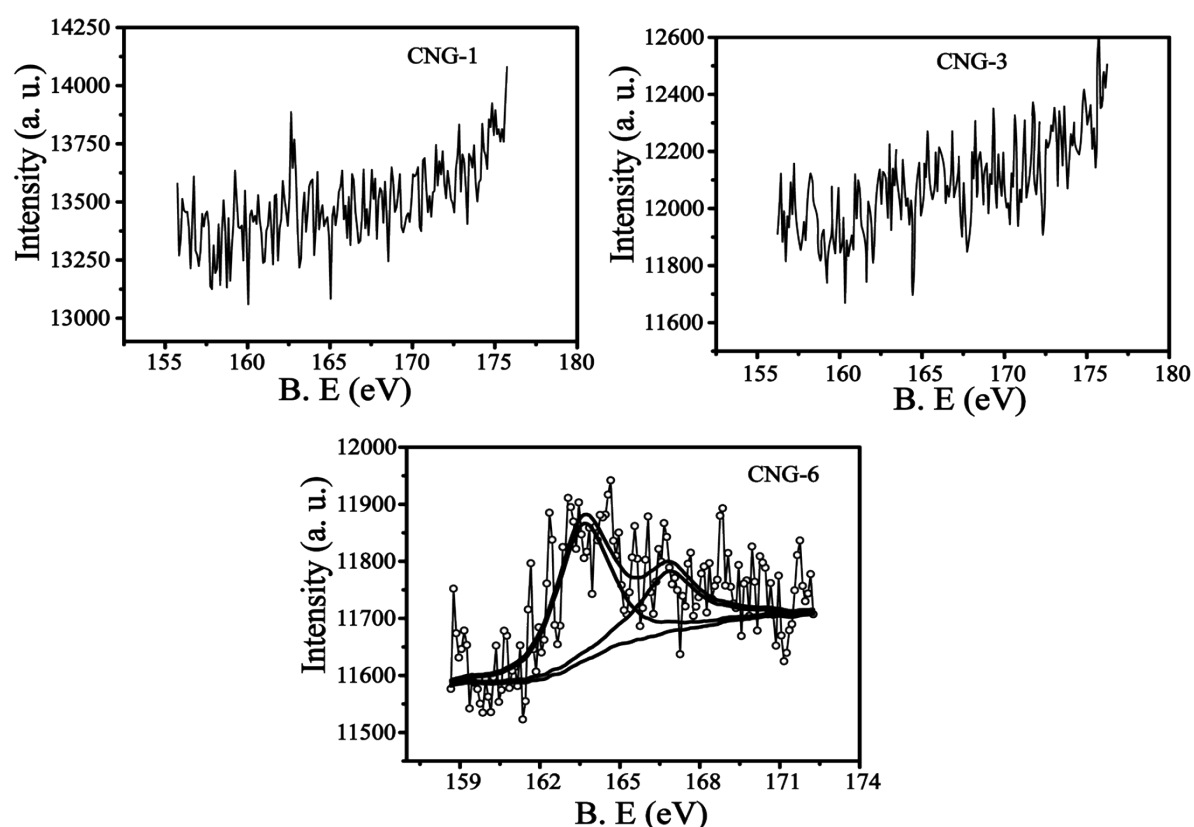


**Figure SI 9.** XPS spectra of sulphur (S) in CNG-1, CNG-3 and CNG-6 samples.

CNG-6 shows presence of 0.95 wt.% of sulphur, which is expected to be generated from MF (**Figure SI 9**). Since the stability of sulphur at high temperature is very poor, it tends to easily escape from the MF during the high temperature annealing process. In the recent literatures, the amounts of sulphur doped in the carbon morphologies are found to be generally less than 1 wt.%.<sup>1</sup> Due to the thin layer wrapping of GO on MF before annealing to generate CNG-1 and CNG-3, sulphur will easily escape from the system at high temperature without

incorporating in the carbon matrix. On the other hand, the presence of large amount of GO sheets in CNG-6 helps entrapment of some sulphur and its subsequent doping in the graphene sheets along with nitrogen atoms.

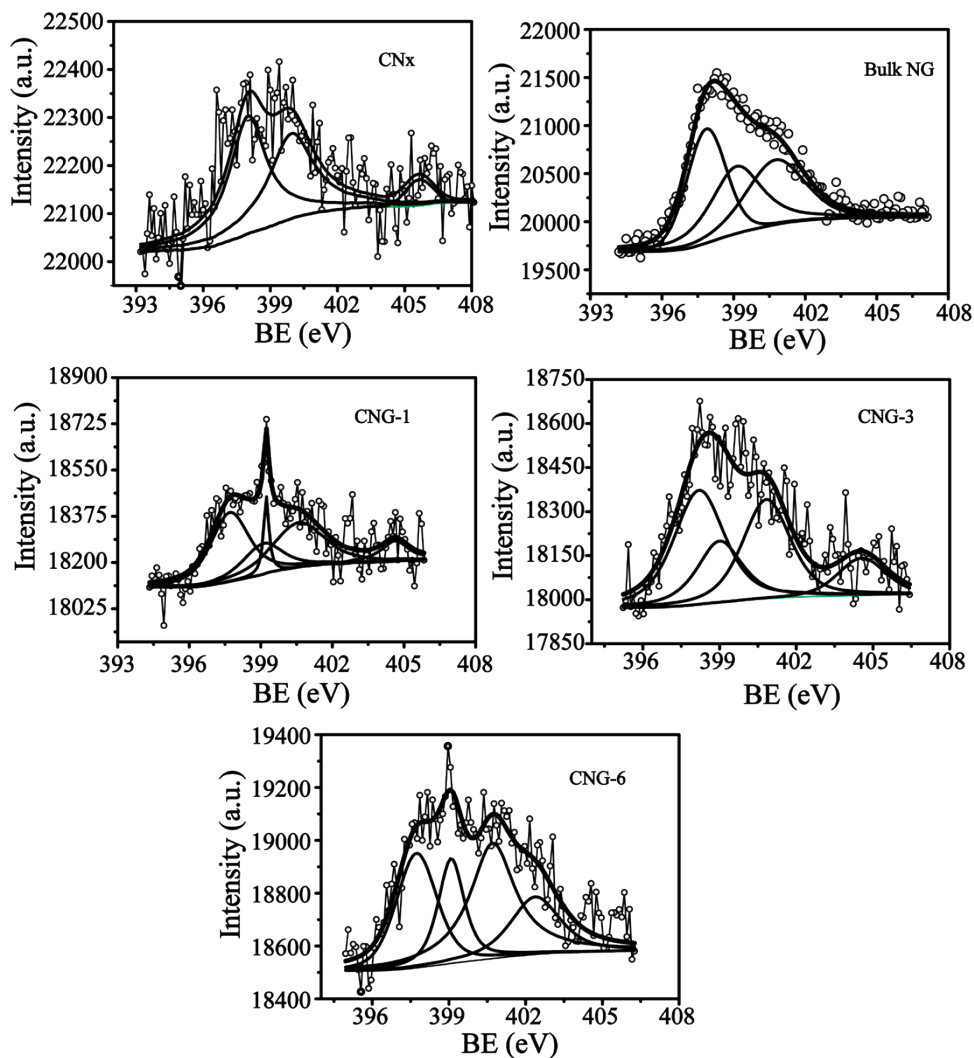


**Figure SI 10.** Deconvoluted XPS spectra of N1s of CN<sub>x</sub>, Bulk NG, CNG-1, CNG-3 and CNG-6.

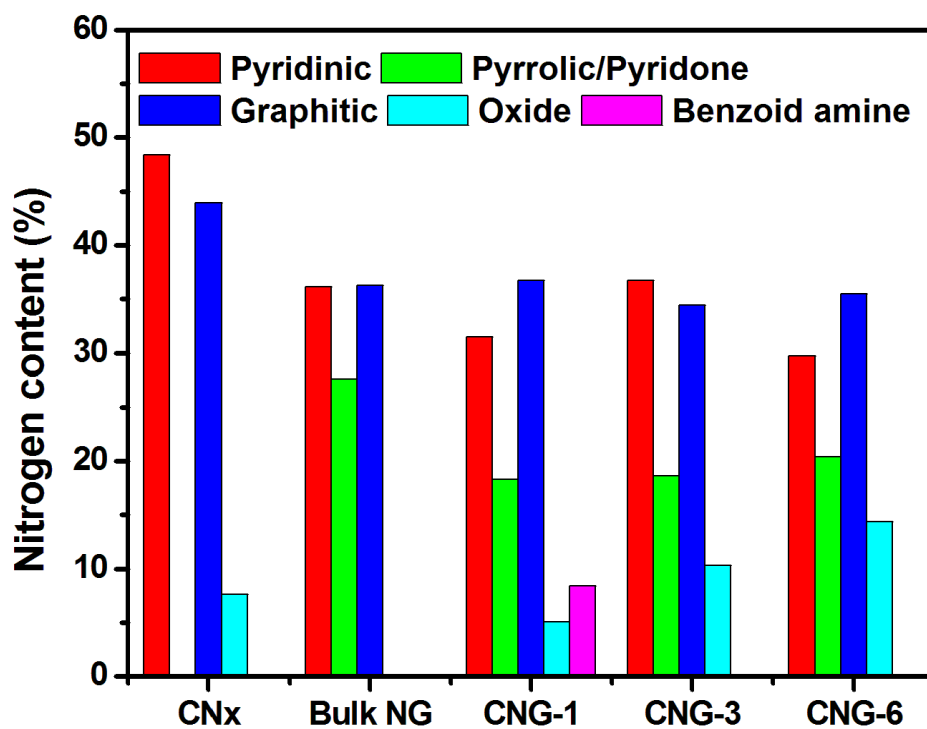


**Figure SI 11.** Percentage of different types of nitrogen content of CN<sub>x</sub>, Bulk NG, CNG-1, CNG-3 and CNG-6.

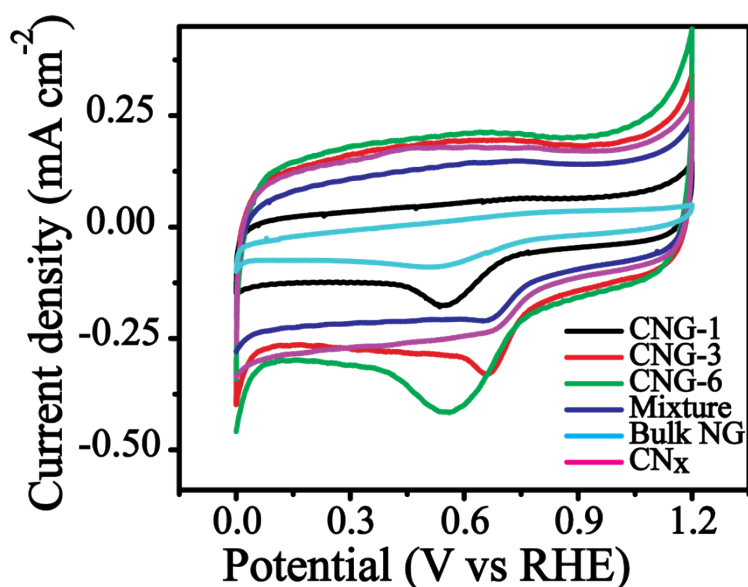


**Figure SI 12.** (a) Cyclic voltammograms of the non-metal catalysts recorded at a scan rate of  $5 \text{ mV s}^{-1}$  in  $0.1 \text{ M HClO}_4$  solution.

Cyclic voltammetry (CV) of all the electrocatalysts was carried out at a scan rate of  $5 \text{ mV s}^{-1}$  in  $0.1 \text{ M HClO}_4$ . For comparing the electrochemical activity of the systems, the testing of the CNG samples was done along with  $\text{CN}_x$ , bulk NG and a physical mixture of the both in a ratio of 1:1 under the similar conditions. In **Figure SI 9**, bulk NG shows a very broad cathodic peak at  $0.59 \text{ V}$  with very low double layer charging current. In contrary, the contribution by double layer charging of  $\text{CN}_x$  is high in association with a cathodic peak shift towards a more positive value of  $0.73 \text{ V}$ . CNG-1 shows capacitance in between Bulk NG and  $\text{CN}_x$  with the cathodic peak at  $0.60 \text{ V}$ . CNG-3 and CNG-6 show high double layer charging contribution compared to CNG-1 and  $\text{CN}_x$  with the cathodic peaks respectively at  $0.72$  and  $0.62 \text{ V}$ . The physical mixture of both  $\text{CN}_x$  and Bulk NG also shows the cathodic peak at a higher potential of  $0.72 \text{ V}$  compared to  $\text{CN}_x$  and bulk NG. CNG-3 and CNG-6 show high capacitive nature compared to Bulk NG. High capacitive nature of CNG-3 and CNG-6 attributes to the peculiar morphology of the catalysts. Three dimensional (3-D) morphology of CNG-3 provides proper channels for mass transport and, hence, help to establish maximum electrode-electrolyte interfaces. At the same time, wrapping of the graphene sheets on the  $\text{CN}_x$  tetrapod units help the system to expose more number of the active reaction sites

for effective dioxygen adsorption and its reduction. These structural benefits obtained from the 3-D morphology of CNG is expected to help the system to shift the reduction peak potential towards more positive side compared to Bulk NG.

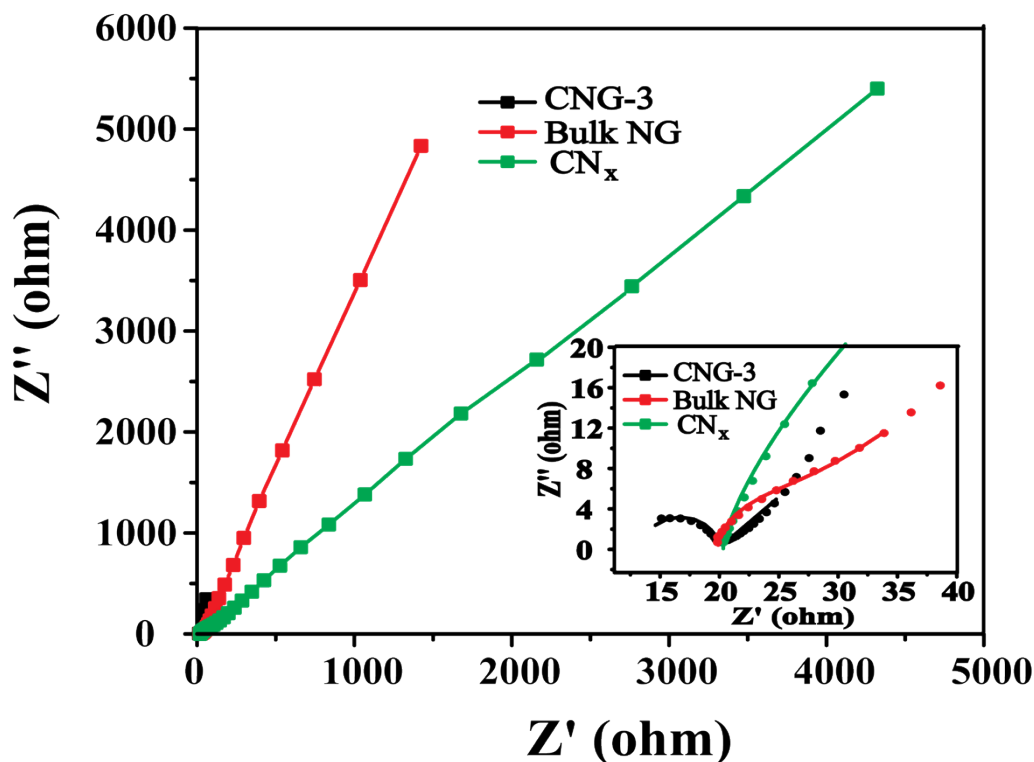


**Figure SI 13.** Nyquist plots of the CN<sub>x</sub>, Bulk NG and CNG-3 recorded in 0.1 M HClO<sub>4</sub> solution with graphite rod and Ag/AgCl as counter and reference electrode respectively. High frequency region is given in the inset of the figure.

From Figure SI 13, it is clear that the resistance of CN<sub>x</sub> is higher than that of bulk NG and CNG-3. The resistance of the materials is found to be in the order of bulk CNG-3 (13.52 Ω) < NG (19 Ω) < CN<sub>x</sub> (20.52 Ω). This indicates that the presence of the graphene sheets around the CN<sub>x</sub> backbone helps for enhancing the electric conductivity of CNG-3.

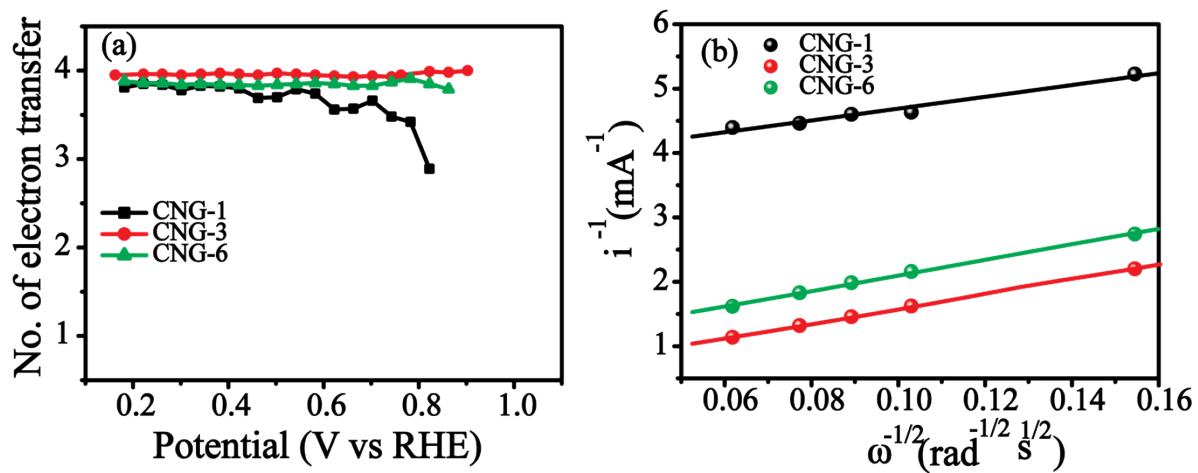


**Figure SI 14.** (a) The plot representing the number of electrons transferred vs. the potential as calculated from RRDE, (b) K–L plots of the CNG electrocatalysts at a potential of 0.34 V vs. RHE.

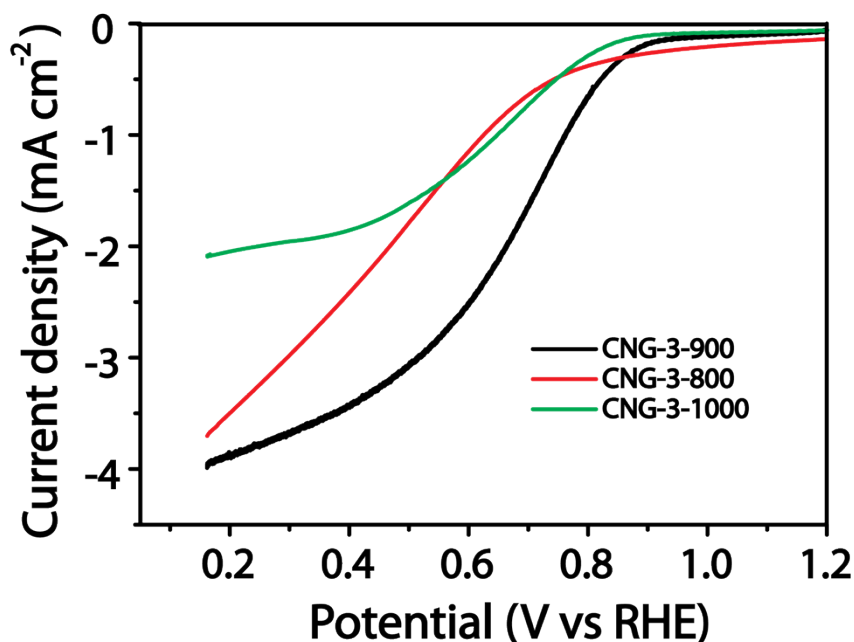


**Figure SI 15.** Linear sweep voltammograms (LSVs) of the CNG-3 samples annealed at different temperatures in 0.1 M oxygen saturated HClO<sub>4</sub> at a rotation speed of 1600 rpm and a scan rate of 5 mV s<sup>-1</sup>. CNG-3 annealed at 800, 900 and 1000 °C are referred CNG-3-800, CNG-3-900 and CNG-3-1000, respectively.

To further understand the effect of annealing temperature on ORR of CNG-3 sample, we also have annealed the sample at 800 and 1000 °C. The corresponding samples are named as CNG-3-800, CNG-3-900, and CNG-3-1000 respectively. It is well known that the annealing temperature can serve as an important parameter in modifying the nitrogen coordination with significant changes in the ORR activity. It can be seen from the figure that CNG-3-900 is showing more positive onset as well as half wave potential compared to CNG-3-800 and CNG-3-1000. It is important to note that reduction current density of CNG-3-1000 has been significantly reduced compared to CNG-3-900 and CNG-3-800. More spectroscopic studies are required to identify the modifications induced in the system in the nitrogen coordinated active sites during the high temperature annealing.

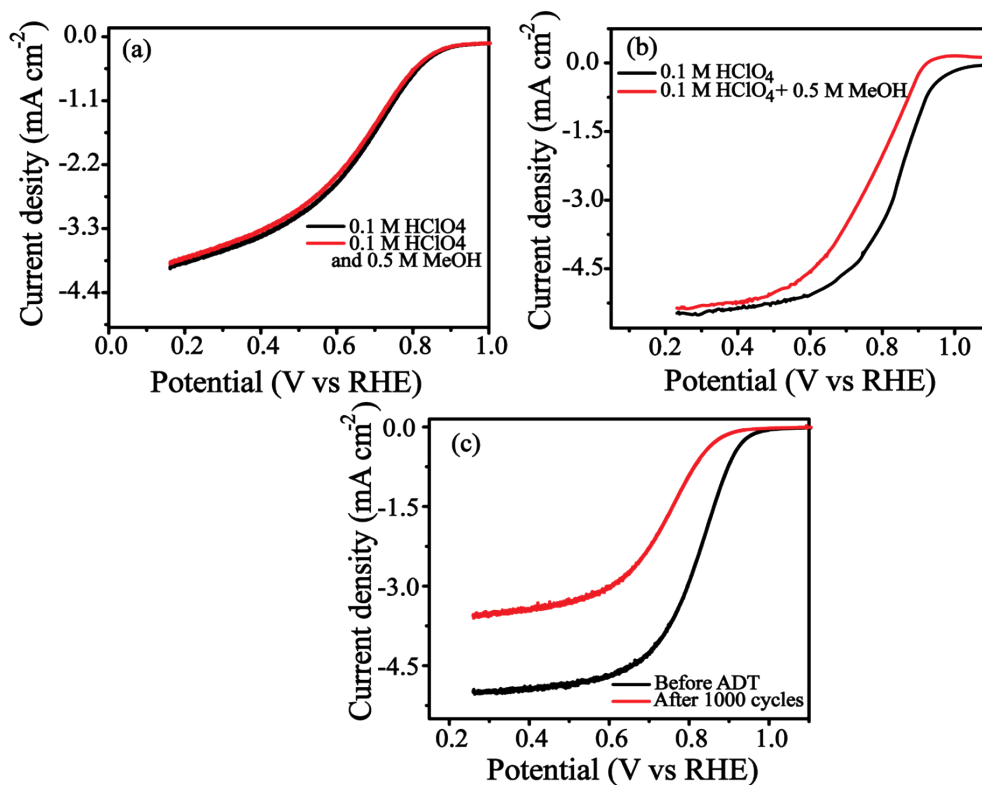


**Figure SI 16.** Methanol crossover study of (a) CNG-3 and (b) Pt/C with an electrode rotation rate of 1600 rpm at a scan rate of 5 mV s<sup>-1</sup>. 0.5 M methanol was added into 0.1 M HClO<sub>4</sub> electrolyte to evaluate the crossover effect and (c) LSVs of Pt/C before and after ADT in oxygen saturated 0.1 M HClO<sub>4</sub> at an electrode rotation speed of 1600 rpm and a scan rate of 5 mV s<sup>-1</sup> respectively.

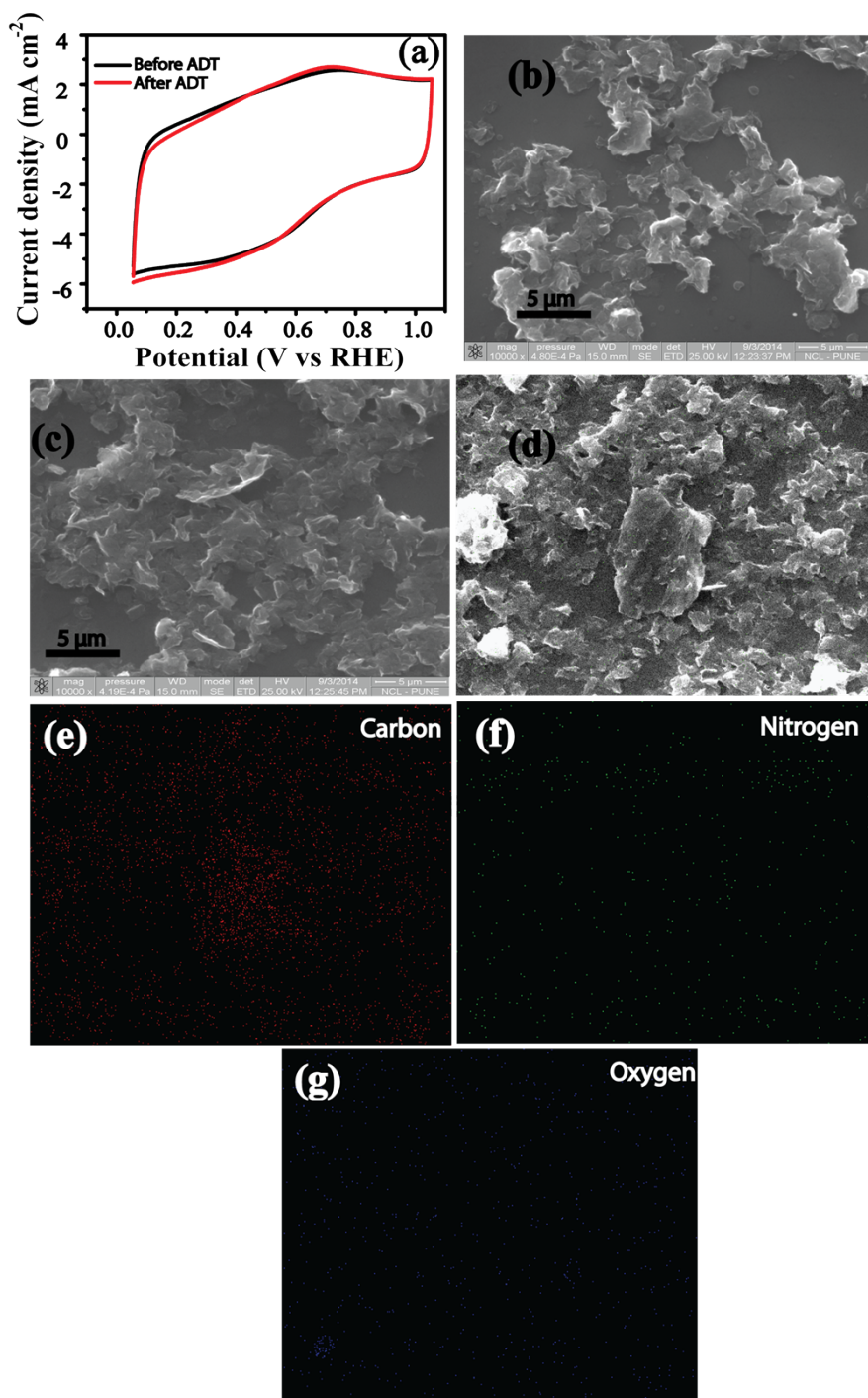


**Figure SI 17.** (a) CV of CNG-3 before and after ADT in oxygen saturated 0.1 M HClO<sub>4</sub> at an electrode rotation speed of 900 rpm and a scan rate of 50 mV s<sup>-1</sup> respectively. (b-d) SEM images of CNG-3 after the durability test and (e), (f) and (g) represent the elemental mapping of carbon, nitrogen and oxygen respectively on CNG-3 after the durability analysis.

To get an insight about the activity enhancement after durability analysis, cyclic voltammetry was performed at 50 mV/s scan rate with an electrode rotation rate of 900 rpm before and after ADT. Interestingly, we did not observe any prominent changes in the voltammogram feature (Figure SI 17 (a)) before and after the durability test. This clearly indicates that quinone type species are not forming due to carbon corrosion during ADT, otherwise it would have given signatures corresponding the redox peak of the species. Similarly, we also have investigated the materials by scanning electron microscopy to find out any possible changes in the morphology of the material after the durability test. From the SEM images (Figure SI 17 (b-d)), it is clear that the morphology is partially collapsed after the 5000 potential cycles. However, we cannot completely conclude that these morphology differences mainly arise from the ADT cycling. Multiple times sonication and drying procedure involved in the sample preparation (for CV followed by the SEM analyses) can also affect the morphology deformation. Since we couldn't completely remove Nafion (the binder used for sticking the catalyst on the electrode) from the catalyst, this also might have played an important role in the structural changes as we observed in the SEM images. Along with the SEM analysis, we have carried out elemental mapping (**Figure SI 17(e-g)**) to understand whether the distribution of nitrogen is getting affected after the durability analysis. From the figure, it is clear that there are no changes in the effective nitrogen distribution on CNG-3 sample after the durability analysis. According to *Zelanay et al (Nat Commun, 2013, 4, 1922)*, higher activity after the durability analysis indicates the formation of more active reaction centres to reduce dioxygen molecule. More detailed research in these direction is one of the main focus in our laboratory. Also, there is a possibility of enhancement in the wettability of the carbon surface under the voltage induced conditions, which may eventually lead to better accessibility of the active centres.

Table SI 1. ORR onset potential and half wave potential of some of the non-metal electrocatalyst recently reported.

		<b>Material</b>	<b>Catalyst loading, scan rate and electrolyte</b>	<b>Onset potential vs RHE</b>	<b>Half wave potential vs RHE</b>	<b>Tafel Slope (mV decade<sup>-1</sup>)</b>
1	Wie <i>et al</i> <sup>[S2]</sup> <i>Angew. Chem. Int. Ed.</i> 2014, 53, 1570	Nitrogen-doped carbon nanosheets	600 $\mu\text{g}/\text{cm}^2$ , 10 mV/s, 0.5 M $\text{H}_2\text{SO}_4$	0.75 V	0.56	unknown
2.	Shi <i>et al</i> <sup>[S3]</sup> <i>J. Mater. Chem. A</i> , 2013, 1, 14853	S and N doped CNT	204 $\mu\text{g}/\text{cm}^2$ , 10 mV/s, 1 M $\text{HClO}_4$	0.75 V	unknown	unknown
3.	Palaniselvam <i>et al</i> <sup>[S4]</sup> <i>Chem. Eur. J.</i> 2013, 19, 9335	ZIF derived carbon	100 $\mu\text{g}/\text{cm}^2$ , 5 mV/s, 0.5 M $\text{HClO}_4$	0.8 V	0.58	unknown
4.	Xiong <i>et al</i> <sup>[S5]</sup> <i>J. Am. Chem. Soc.</i> 2010, 132, 15839	3D CNT	Not given, 5 mV/s, 3 M $\text{H}_2\text{SO}_4$	unknown	unknown	unknown
5.	Ding <i>et al</i> <sup>[S6]</sup> <i>Angew. Chem. Int. Ed.</i> 2013, 52, 11755	Pyridinic and pyrrolic nitrogen doped graphene	600 $\mu\text{g}/\text{cm}^2$ , 10 mV/s, 0.5 M $\text{H}_2\text{SO}_4$	0.895V	unknown	unknown
6	Yu <i>et al</i> <sup>[S7]</sup> <i>J. Am. Chem. Soc.</i> 2010, 132, 15127	NCNT	Unknown 10mV/s, 0.5 M $\text{H}_2\text{SO}_4$	0.62 V	0.44 V	unknown
7	<b>Present work</b>	<b>CNG-3</b>	<b>255 <math>\mu\text{g}/\text{cm}^2</math>, 5 mV/s, 0.1M <math>\text{HClO}_4</math></b>	<b>0.89</b>	<b>0.68</b>	<b>109</b>

- S1. a) Z. Yang, Z. Yao, G. Li, G. Fang, H. Nie, Z. Liu, X. Zhou, X. a. Chen and S. Huang, *ACS Nano*, 2011, **6**, 205-211; b) S. Some, Y. Kim, Y. Yoon, H. Yoo, S. Lee, Y. Park and H. Lee, *Sci. Rep.*, 2013, **3**.
- S2. W. Wei, H. Liang, K. Parvez, X. Zhuang, X. Feng and K. Müllen, *Angew. Chem. Int. Ed.*, 2014, **53**, 1570-1574.
- S3. Q. Shi, F. Peng, S. Liao, H. Wang, H. Yu, Z. Liu, B. Zhang and D. Su, *J. Mater. Chem. A*, 2013, **1**, 14853-14857.
- S4. T. Palaniselvam, B. P. Biswal, R. Banerjee and S. Kurungot, *Chemistry – A European Journal*, 2013, **19**, 9335-9342.
- S5. W. Xiong, F. Du, Y. Liu, A. Perez, M. Supp, T. S. Ramakrishnan, L. Dai and L. Jiang, *J. Am. Chem. Soc.*, 2010, **132**, 15839-15841.
- S6. W. Ding, Z. Wei, S. Chen, X. Qi, T. Yang, J. Hu, D. Wang, L.-J. Wan, S. F. Alvi and L. Li, *Angew. Chem. Int. Ed.*, 2013, **52**, 11755-11759.
- S7. D. Yu, Q. Zhang and L. Dai, *J. Am. Chem. Soc.*, 2010, **132**, 15127-15129.